Carbohydrate Polymers 152 (2016) 548–557

Contents lists available at ScienceDirect

Carbohydrate Polymers

journal homepage: www.elsevier.com/locate/carbpol

Halloysite nanotubes loaded with peppermint essential oil as filler for functional biopolymer film

G. Biddeci[a], G. Cavallaro[b,*], F. Di Blasi[a], G. Lazzara[b], M. Massaro[c,*], S. Milioto[b], F. Parisi[b], S. Riela[c], G. Spinelli[a]

[a] Institute of Biomedicine and Molecular Immunology, CNR, IBIM, Via Ugo La Malfa, 153, 90146 Palermo, Italy
[b] Department of Physics and Chemistry, University of Palermo, Viale delle Scienze, Ed. 17, Palermo, Italy
[c] Department STEBICEF, Sect. Chemistry, University of Palermo, Viale delle Scienze, Ed. 17, 90128 Palermo, Italy

ARTICLE INFO

Article history:
Received 16 May 2016
Received in revised form 28 June 2016
Accepted 11 July 2016
Available online 12 July 2016

Dedicated to the 70th birthday of Prof. Renato Noto

Chemical compounds studied in this article:
Halloysite nanotubes (PubChem CID: 6337008)
Cucurbit[6]uril (PubChem CID: 196163)
Pectin (PubChem CID: 441476)
Peppermint essential oil (PubChem CID: 6850741)
Menthone (PubChem CID: 26447)
DPPH (PubMed CID: 2735032)

Keywords:
Halloysite nanotubes
Nanocomposite food packaging
Essential oil
Pectin
Antimicrobial and antioxidant properties

ABSTRACT

The purpose of this paper is to show how a functional bionanocomposite film with both antioxidant and antimicrobial activities was successfully prepared by the filling of a pectin matrix with modified Halloysite nanotubes (HNT) containing the essential peppermint oil (PO). Firstly, HNT surfaces were functionalized with cucurbit[6]uril (CB[6]) molecules with the aim to enhance the affinity of the nanofiller towards PO, which was estimated by means of HPLC experiments. The HNT/CB[6] hybrid was characterized by several methods (thermogravimetry, FT-IR spectroscopy and scanning electron microscopy) highlighting the influence of the supramolecular interactions on the composition, thermal behavior and morphology of the filler. Then, a pectin + HNT/CB[6] biofilm was prepared by the use of the casting method under specific experimental conditions in order to favor the entrapment of the volatile PO into the nanocomposite structure. Water contact angle measurements, thermogravimetry and tensile tests evidenced the effects of the modified filler on the thermo-mechanical and wettability properties of pectin, which were correlated to the microscopic structure of the biocomposite film. In addition, PO release in food simulant solvent was investigated at different temperatures (4 and 25 °C), whereas the antioxidant activity of the nanocomposite film was estimated using the DPPH method. Finally, we studied the in vitro antibacterial activity of the biofilm against *Escherichia coli* (Gram-negative) and *Staphylococcus aureus* (Gram-positive), which were isolated by beef and cow milk, respectively. These experiments were carried out at specific temperatures (4, 37 and 65 °C) that can be useful for a multi-step food conservation. This paper puts forwards an easy strategy to prepare a functional sustainable edible film with thermo-sensitive antioxidant/antimicrobial activity.

1. Introduction

In recent years, foodborne diseases are among the most public health issues worldwide. Essential oils derived from different natural sources, such as rosemary, oregano, thyme and peppermint (PO), are efficient additives for food preservation because of their antimicrobial properties toward several foodborne pathogens (Burt, 2004). Contrary to the standard preservation procedures (heating, cooling and addition of chemical compounds), the addition of essential oils does not alter the organoleptic characteristic of food. Because of their hydrophobic nature the essential oils can penetrate the lipid layers of the bacterial cell membrane disturbing its structures (Bakry et al., 2016). Furthermore, essential oils are categorized as GRAS (Generally Recognized as Safe) by U.S. Food and Drug Administration allowing them to be used in the food industry without further approval (Arfat, Benjakul, Prodpran, Sumpavapol, & Songtipya, 2014; Manso, Becerril, Nerín, & Gómez-Lus, 2015).

Recently, active packaging based on biocompatible films has attracted growing interest due to concerns for the environment (Garcıía, Pinotti, Martino, & Zaritzky, 2004). Edible biofilms are commonly composed by sustainable polymers, such as chitosan (Beverlya, Janes, Prinyawiwatkula, & No, 2008), starch (Talja, Peura, Serimaa, & Jouppila, 2008), cellulose (Cavallaro, Donato, Lazzara, & Milioto, 2011) and pectin (Espitia, Du, Avena-Bustillos, Soares, & McHugh, 2014).

* Corresponding authors.
E-mail addresses: giuseppe.cavallaro@unipa.it (G. Cavallaro), marina.massaro@unipa.it (M. Massaro).

http://dx.doi.org/10.1016/j.carbpol.2016.07.041
0144-8617/

Pectin possesses a complex hetero-polysaccharide structure containing linear and branched regions, constituted by poly α-1,4-galacturonic acids. Pectin-based packaging usually does not reflect the physical advantageous properties of conventional packaging limiting their practical applications (Sorrentino, Gorrasi, & Vittoria, 2007). Filling the polymer matrix with plasticizers (Cavallaro, Lazzara, & Milioto, 2013), emulsifiers or clay (Alcantara, Aranda, Darder, & Ruiz-Hitzky, 2010; Espitia et al., 2014) determined an improvement to the physico-chemical performances of pectin based films.

A pectin/starch blend showed relevant mechanical properties (Coffin, Fishman, & Ly, 1996) as well as excellent oxygen barrier capability (Coffin & Fishman, 1994). Composite films based on gelatin and pectin evidenced better tensile characteristics and water resistance than the pristine polymers (Farris et al., 2011). The addition of nanoclays (Ali, Tang, Alavi, & Faubion, 2011; Cavallaro et al., 2013; Cavallaro, Lazzara, & Milioto, 2011) generated an enhancement of the pectin thermal stability.

Among the clay nanoparticles, halloysite nanotubes (HNT) are an emerging nanofiller as a consequence of their hollow tubular morphology and tunable surface chemistry (Pasbakhsh, Churchman, & Keeling, 2013). Halloysite is a biocompatible material as shown by several in vitro and in vivo studies (Bellani et al., 2016; Fakhrullina, Akhatova, Lvov, & Fakhrullin, 2015; Kryuchkova, Danilushkina, Lvov, & Fakhrullin, 2016; Massaro, Piana et al., 2015). The HNT length ranges between 0.2 and 1.5 μm, while the inner and the outer diameters are ca. 10–30 nm and 40–70 nm, respectively (Abdullayev & Lvov, 2013). Halloysite possesses a positive alumina inner lumen and a negative silica outer surface allowing its selective functionalization (Arcudi et al., 2014; Cavallaro, Lazzara, & Milioto, 2012), the formation of a liquid crystalline phase (Luo et al., 2013) and the encapsulation of chemically and biologically active compounds (Abdullayev et al., 2011; Lvov, Shchukin, Möhwald, & Price, 2008; Lvov & Abdullayev, 2013; Lvov, Wang, Zhang, & Fakhrullin, 2016; Lvov, DeVilliers, & Fakhrullin, 2016; Shutava, Fakhrullin, & Lvov, 2014;), such as drugs (Aguzzi, Cerezo, Viseras, & Caramella, 2007; Lun, Ouyang, & Yang, 2014), natural molecules (Massaro, Piana et al., 2015), marine biocides (Wei et al., 2014), cosmetics (Suh et al., 2011), and other functional agents (Abdullayev, Price, Shchukin, & Lvov, 2009). HNT are suitable as catalytic supports (Machado, de Freitas Castro, Wypych, & Nakagaki, 2008; Massaro et al., 2014; Massaro, Riela et al., 2015), adsorbent nanomaterials for wastewater decontamination (Szczepanik & Słomkiewicz, 2016; Zhang et al., 2016), and nanofiller for sustainable packaging (Liu, Wu, Jiao, Xiong, & Zhou, 2013; Tescione, Buonocore, Stanzione, Oliviero, & Lavorgna, 2014). Research reports (Gorrasi, 2015; Lee & Park, 2015) that pristine HNT exhibited an excellent essential oils solubilization ability as well as controlled release of properties. In addition, HNT loaded with essential oils were successfully used as nanofiller for polymers (Gorrasi, 2015; Lee & Park, 2015) making the obtained composite biofilms appropriate for packaging applications. HNT improve physical barrier properties of polymeric materials such as poor barrier properties to water vapor (Sorrentino et al., 2007).

Herein, we have developed a novel biodegradable film based on pectin reinforced with functionalized HNT containing essential peppermint oil. In particular, supramolecular interactions between HNT surfaces and cucurbit[6]uril (CB[6]) molecules endowed to synthesize a hybrid nanofiller with high solubilization capacity towards the essential oils.

The CB[6] was selected for its interesting distinctive abilities to bind molecules both with its hydrophobic cavity and its ureido carbonyl rim by hydrogen-bonding interactions (Márquez, Hudgins, & Nau, 2004). The "multi-pocket" HNT/CB[6] filler could enhance the pristine HNT ability to entrap PO on the CB[6] cavity and, at the same time, it could improve the pectin barrier properties to water vapor by hydrogen-bonding interactions with the macrocyclic molecules adsorbed on the HNT external surface.

An alternative casting method to fill the bionanocomposites with PO was developed. An extensive characterization of the film was carried out including the determination of thermal, structural, mechanical and functional properties (antioxidant and antimicrobial activities). In particular, we performed in vitro tests on two bacteria directly isolated from beef (*Escherichia coli*) *and* cow milk (*Staphylococcus aureus*).

Noteworthy, the prepared functional film is composed of ecocompatible molecules (pectin, CB[6] and essential oil), which are sketched in Fig. 1. Accordingly, the nanocomposite might be considered as a biocompatible material for packaging applications.

2. Experimental section

2.1. Materials

Pectin (degree of methyl esterification, 24%, MW: 100 kg mol^{-1}), halloysite nanotubes and all reagents needed were purchased from Sigma-Aldrich and used without further purification. Cucurbit[6]uril was synthesized through the procedure reported by Kim et al. (2000) Peppermint essential oil was purchased from AromaZone.com.

2.2. Methods

2.2.1. Contact angle measurements

Contact angle studies were performed by means of an optical contact angle apparatus (OCA 20, Data Physics Instruments) equipped with a video measuring system having a high-resolution CCD camera and a high-performance digitizing adapter. SCA 20 software (Data Physics Instruments) was used for data acquisition. Rectangular (5 cm × 2 cm) films were fixed on top of a plane solid support and kept flat throughout the analysis. The contact angle (θ) of water in air was measured using the sessile drop method by gently placing a droplet of 6 ± 0.5 mL onto the surface of the film. Temperature was set at 25.0 ± 0.1 °C both for the support and the injecting syringe. Images were collected 25 times per second, starting from the deposition of the drop to 60 s. Five experiments were performed on each film sample, and the average values are reported.

2.2.2. FTIR

Spectra were recorded with an Agilent Technologies Cary 630 FTIR spectrometer. Specimens for measurements were prepared by mixing 5 mg of the sample powder with 100 mg of KBr.

2.2.3. Thermogravimetry analysis (TGA)

Experiments were done using the instrument Q5000 IR (TA Instruments) under nitrogen flow (25 cm^3 min^{-1}) by heating the samples from room temperature to 900 °C. Each sample (4–10 mg) was placed in a platinum pan and heated under the temperature program of 20 °C min^{-1}. The polymer degradation temperature was estimated from the peak of differential thermogravimetric (DTG) curves in the range between 200 and 400 °C.

2.2.4. Differential scanning calorimetry (DSC)

Experiments were performed by using a differential scanning calorimeter TA Instrument DSC (2920 CE). The calorimeter was calibrated using indium as standard. Each sample (2–3 mg) was heated according to a temperature program of 10 °C min^{-1} in the range comprised between 10 and 500 °C.

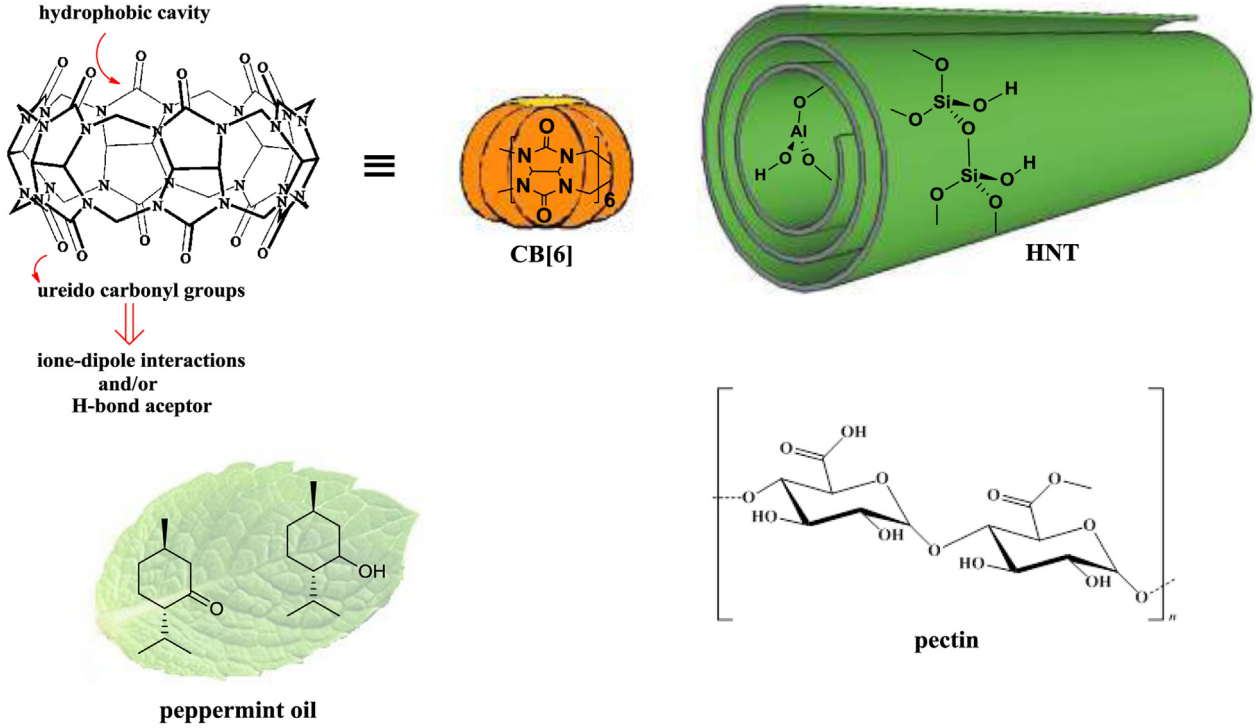

Fig. 1. Schematic representation of the pectin films components.

2.2.5. Scanning electron microscopy

The microscope ESEM FEI QUANTA 200F was used to study the morphology of the functionalized HNT. Before each experiment, the sample was coated with gold in argon by means of an Edwards Sputter Coater S150A to avoid charging under electron beam.

2.2.6. Dynamic mechanical analysis

Tensile properties were determined by means of a DMA Q800 instrument (TA Instruments). For all mechanical measurements, the samples were films of rectangular shape (10.00 mm × 6.00 mm × 0.120 mm), while tensile tests were performed with a stress ramp of 1 MPa min^{-1} at 26.0 ± 0.5 °C. We determined the values of the elastic modulus, which was calculated by the slope of the linear region in the stress vs strain curve. In addition, we estimated the tensile strength (defined as the tensile stress at which the material fractures), and the elongation at the breaking point. Each nanocomposite was measured five times, and the average values are reported.

2.2.7. Water uptake

The water uptake (WU) experiments were carried out on 5 specimens of the pectin + HNT/CB[6] composite with the same size used for DMA measurements. Samples were first dried under vacuum at 25 °C for ca. 2 h. Afterwards, the films were placed in hermetic chambers containing oversaturated NaCl solution in order to maintain the relative humidity (RH) at a constant level of 75%. The temperature of hermetic chambers was set at 25.0 ± 0.5 °C. The films were weighted after two weeks conditioning at certain RH% endowing to calculate the WU% as follows:

$$WU\% = 100 \times \left(\frac{M_f - M_i}{M_f} \right) \quad (1)$$

where M_i and M_f are the weights before and after two weeks exposure to 75% RH. The obtained WU% value (calculated as average of the 5 specimens) was compared to that of pristine pectin (Cavallaro et al., 2013).

2.2.8. HPLC investigations

The chromatographic measurements were performed using a Shimadzu Class VP (Shimadzu, Japan), which consist of a pump (LC-10AD VP Shimadzu), an injection valve equipped with a 20 mL injection loop, UV–vis Diode-Array (SPD-M10A VP) detector and an acquisition data software Class-VP. After optimization of the chromatographic conditions, separation was carried out on C_{18} column (Discovery Supelco, 25 cm, 4.6 mm, 5 mm). The mobile phase consisted of 100% methanol, at room temperature, in 1 mL min^{-1} flow. Chromatograms were analyzed at 276 nm.

2.2.9. Transmission electron microscopy

Micrographs were acquired with a Jeol JEM 2100 microscope operating at 200 kV. A drop of each dispersion was deposited in a 3 mm nickel grid holey carbon coated (Taab). The grid was dried overnight before observation. No coating was applied for the observation.

2.3. Preparation of HNT/CB[6] hybrid

The HNT/CB[6] supramolecular structure was prepared as described in the literature (Massaro, Riela et al., 2016). Briefly, aqueous saturated CB[6] solution (0.018 mmol L^{-1}) was mixed with halloysite powder and sonicated for 15 min. Then, the obtained suspension was stirred and kept under vacuum for 3–5 min resulting in light fizzling and the loaded compound condensated within the tube. This procedure was repeated three times to improve the loading efficiency. Successively, the sample was separated from the aqueous phase by centrifugation and free cucurbituril was isolated and recycled for further experiments. The complex HNT/CB[6] was washed several times with water, and dried under vacuum at 70 °C overnight.

2.4. Loading of peppermint essential oil into HNT/CB[6] hybrid

In a 25 mL round bottom flask 30 mg of HNT/CB[6] hybrid and ca. 100 mg of peppermint essential oil (PO) were weighed and 1 mL

of water was added. The dispersion was left to stir at room temperature overnight. Then, the solvent was filtered off and the solid rinsed with 25 mL of water. The filtrate was analyzed by HPLC to quantify the essential oil loading on HNT/CB[6] using a calibration curve. The amount of oil loaded into the hybrid was expressed as the percentage of PO in the obtained composite.

2.5. Preparation of bionanocomposite

Firstly, a 2 wt% aqueous pectin solution was prepared and it was left to stir at room temperature overnight. Then, 30 mg of HNT/CB[6] or HNT/CB[6]/PO were added to the pectin solution and kept under stirring for ca. 6 h. For the bionanocomposite with HNT/CB[6] as filler, the well-dispersed aqueous mixture was poured into glass Petri dishes at 60 °C to evaporate water until the weight was constant. Dried biofilms contained 5 wt% of nanofiller. Contrary to this, the bionanocomposite with PO was prepared by pouring the well-dispersed aqueous mixture into glass Petri and then it was left at room temperature and under vacuum in a chamber in the presence of silica and P_2O_5, which were freshly added during the course of experiment. The described preparation procedure was efficient as evidenced by the compact mechanical features of the obtained bionanocomposite film. In addition, no voids or craters were observed on the film surface.

2.6. Peppermint oil release from films into food simulant

The release of the active components of peppermint essential oil from the bionanocomposite into a food simulant was carried out at 4 °C and at room temperature. 50% v/v ethanol as simulant for food with lipophilic character (D1) was selected according to the European Regulations. For the release experiments, 2 × 2 cm film samples were immersed in 1 mL of simulant in sealed vials and in the dark. At various selected times, films were removed from the sample and the liquid stored at 4 °C for the subsequent chromatographic analysis. The concentration of one of the main compound (menthone) was analysed by HPLC using a calibration curve.

2.7. Antioxidant activity of bionanocomposites

The antioxidant properties were evaluated using the 2,2-diphenyl-1-picrylhydrazyl radical (DPPH•) method. This radical is commonly used to evaluate the antioxidant properties of natural products, as the purple free radical is transformed by reductants to the yellow hydrazine through a formal hydrogen atom transfer reaction. The interaction of PO with DPPH radicals resulted in fast decoloration of the DPPH solution. Radical scavenging activity was determined following a procedure reported in literature (Iturriaga, Olabarrieta, Castellan, Gardrat, & Coma, 2014). A stock solution of PO (30.0 mg mL^{-1}) was made up in ethanol 50% (v/v) and then diluted to prepare the concentration series for PO antioxidant capacity determination. One mL of DPPH solution (1.5×10^{-4} M) in 50% v/v ethanol was added to 1.0 mL of the tested sample. The mixture was then vigorously mixed and allowed to stand at room temperature in the dark for 60 min. The inhibition of free radical DPPH in percent (I%) was calculated as:

$$I\% = \left(\frac{A_c - A_{PO}}{A_c}\right) \times 100 \quad (2)$$

where A_c is the absorbance of the DDPH solution without PO (λ = 523 nm), and A_{PO} is the absorbance of the test sample. All tests were carried out in duplicate, and inhibition percentages were reported as mean ± SD. The inhibition percentage of the released PO solution was determined after 120 h of immersion of the film into the food simulant.

2.8. Culture strains

Escherichia coli and *Staphylococcus aureus* (isolated from food sources, a generous gift of Dr. Chiara Piraino of Istituto Zooprofilattico Sperimentale della Sicilia) were maintained by regular subculture on Luria Bertani agar (LB agar 35 g/L, affymetrix-USB) for *E. coli* and Blood Agar with 5% Sheep Blood (BD) for *S. aureus*, preserved at 4 °C and transferred monthly.

2.9. Antimicrobial activity of bionanocomposites against E. coli and S. aureus

Films with and without peppermint oil were subjected to various temperature treatments: 30 min at 4 °C, 30 min at 37 °C and 30 min at 65 °C, reproducing the food preservation process. Before starting, each strain was smeared on agar in order to obtain single colonies and incubated at 37 °C for 24 h. A single colony was transferred to 10 mL of Luria Bertani broth (LB broth 20 g/L, affymetrix-USB) for *E. coli* and to 10 mL of Brain Heart Infusion (BHI medium 37 g/L, BD) for *S. aureus* and grown in a shaker at 37 °C 220 rpm for 18 h to obtain cells in a stationary phase. Then 100 μL of each culture strain in stationary phase were diluted in 10 mL of a respective fresh medium and grown in a shaker at 37 °C 220 rpm until exponential phase ($OD_{600} \leq 0.2$), which was verified by measuring the optical density at 600 nm. 0.1 g/5 mL of each film sample were placed in 50 mL falcon tubes with LB for *E. coli* and BHI for *S. aureus* and subjected to treatments at different temperatures. The bionanocomposites film, without peppermint oil, were used as a control. After the different treatments, the medium with films was allowed to reach room temperature. Then 100 μL of cell cultures, with an optical density of 0.2 at 600 nm, were added to tubes with films. Each tube was incubated at 37 °C and 220 rpm until the end of the exponential phase. Serial dilutions with fresh medium were carried out and plated in LB agar for *E. coli* and Blood Agar with 5% Sheep Blood for *S. aureus*. Plates were incubated at 37 °C for 24 h. All analyses were carried out in triplicate. Colonies were counted and the results expressed as% bacterial viability.

2.10. Statistical analysis

All the experiments were performed in triplicate and repeated at least twice. The average values with standard deviations were used for statistical analysis. GraphPad software was used to analyze the resulting data and *t*-Student Test was used to determine the significant differences at a 99% confidence interval, at least.

3. Results and discussion

3.1. HNT/CB[6] hybrid: properties and oil solubilization ability

The HNT/CB[6] filler was prepared according to a procedure reported elsewhere for a similar nanohybrid (Massaro, Riela et al., 2016). FTIR data evidenced the successful functionalization of halloysite surfaces being that the spectrum of the HNT/CB[6] hybrid presents the characteristic vibration bands of both components (Fig. 2).

Compared to pristine HNT, the hybrid showed the OH stretching vibration bands of the Al-OH at lower frequencies (3697 and 3624 cm^{-1}) as a consequence of the interactions between the CB[6] portal carbonyl groups and the HNT inner surface (via hydrogen bonds formation Al—OH···O═C—). Accordingly, the C═O stretching vibration band of the CB[6] adsorbed onto HNT surfaces was shifted to a lower value (1733 cm^{-1}) with respect to that observed for pristine CB[6] (1748 cm^{-1}). Moreover, the successful functionalization of HNT surfaces was highlighted by the presence of the CH_2 stretching vibration bands (2998 and 2929 cm^{-1}) in the hybrid material.

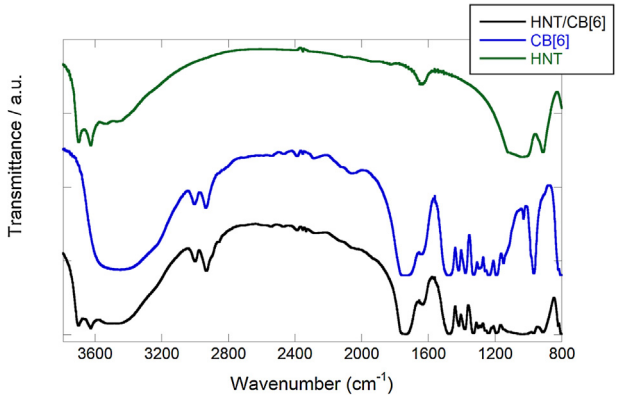

Fig. 2. FT-IR spectra for HNT, CB[6] and HNT/CB[6] hybrid.

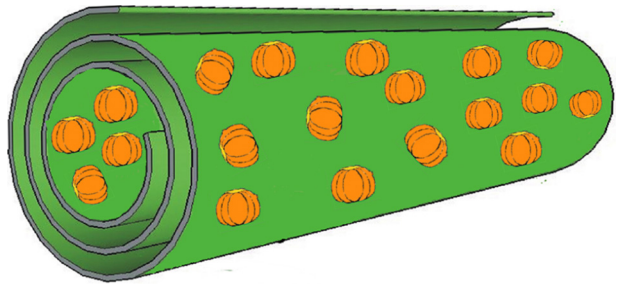

Fig. 3. Cartoon representation of the *inter* and *intra* lumen supramolecular interaction between CB[6] and HNT.

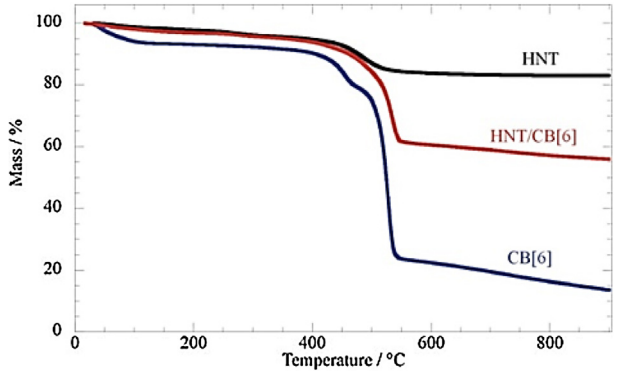

Fig. 4. Thermogravimetric curves of CB[6], HNT and CB[6]/HNT.

These values are lower than those of the pristine CB[6] (3002 and 2934 cm^{-1}). A similar effect was evidenced for the cetyltrimethyl ammonium bromide adsorption onto HNT (Cavallaro et al., 2012) and montmorillonite (Zhu, He, Zhu, Wen, & Deng, 2005) and it was related to the high packing density of organic moiety at the interface. Accordingly, the shifting of the stretching bands could be ascribed to the electrostatic interactions between the positively alumina groups of HNT inner surface and the dipole of carbonyl groups of CB[6] as sketched in Fig. 3.

A quantitative analysis of TG curves (Fig. 4) endowed to estimate the hybrid composition (39 and 61 wt% for CB[6] and HNT, respectively), which clearly reveals the high efficiency of the halloysite functionalization. Based on the geometric volume of the nanotube cavity it was reported that ca. 10% of the void space is available for encapsulation (Lvov et al., 2008). On this basis, we concluded that CB[6] is adsorbed both on the HNT inner and outer surfaces as confirmed by FTIR data (Figs. 2 and 3).

It should be noted that the weight signal change of the hybrid is slightly influenced by the typical halloysite weight loss occurring at ca. 550 °C (Fig. 4), which is attributed to the expulsion of two water molecules from the HNT interlayer (Cavallaro, Lazzara et al., 2011). In addition, both pristine components and the HNT/CB[6] composite exhibited a mass loss between 25 and 150 °C that is correlated to the physically adsorbed water (Fig. 4) (Cavallaro, Lazzara et al., 2011). Due to the presence of CB[6], the modified HNT possess a larger water content (2.7 wt%) with respect to that observed for the pristine ones (1.7 wt%).

As concerns the morphological features, SEM images evidenced that the halloysite tubular shape is preserved in the functionalized HNT. Additionally, the HNT/CB[6] hybrid showed a rather compact structure where the nanotubes seem glued together (Fig. 5).

TEM images were collected for HNT and HNT/CB[6] hybrid (see ESI). The hollow cavity is still present in the modified nanotubes, this finding indicates that either the lumen is only partially filled up or the incorporated CB[6] does not provide enough contrast.

Loading experiments of peppermint oil (PO) revealed that the HNT functionalization with CB[6] represents an efficient route to prepare hybrid nanomaterials with a high solubilization ability towards a volatile organic compound. HPLC experiments evidenced that the addition of CB[6] onto the HNT surfaces determines a relevant increase of the PO loading efficiency (7 and 60 wt% for HNT and HNT/CB[6]). Accordingly, DSC curves (see ESI) of both nanomaterials loaded with the essential oil exhibited an endothermic peak at ca. 70 °C, which is correlated to the PO evaporation. We observed that the enthalpy value is significantly larger for HNT/CB[6]/PO in agreement with the enhanced solubilization ability towards PO induced by the HNT modification. These results confirmed that the multi-macrocyclic receptors adsorbed onto the HNT surfaces are a proper nanocontainer for volatile hydrocarbons, such as essential oils. On this basis, HNT/CB[6]/hybrid was used as a filler to prepare nanocomposite films with antioxidant and antimicrobial properties.

3.2. Bionanocomposite films

3.2.1. Characterization of pectin + HNT/CB[6] nanocomposite

A preliminary physico-chemical characterization of the bionanocomposite film based on pectin and HNT/CB[6] was carried out in order to evaluate its potential use in food packaging. The filling of the polymer with HNT/CB[6] determined a slight enhancement of the surface hydrophobicity as evidenced by the initial water contact angle values, which are $76 \pm 2°$ (Cavallaro, Donato et al., 2011) and $82 \pm 3°$ for pristine pectin and pectin/HNT/CB[6] nanocomposite, respectively. Marmur stated that the addition of hydrophilic substances can generate hydrophobic surfaces if the roughness is enhanced (Marmur, 2008).

As concerns the investigated bionanocomposite, the tendency of HNT/CB[6] hybrid to form clusters of micrometer size (Fig. 5) can generate an increase of pectin surface roughness. Literature reports that the films wettability influences the capacity of biomaterials to adsorb water from environmental moisture (Cavallaro et al., 2013; Průšová, Šmejkalová, Chytil, Velebný, & Kučerík, 2010). Within this, we observed a WU% enhancement induced by the HNT/CB[6] filling into the pectin matrix confirming the hydrophilic nature of modified HNT. After conditioning the RH = 75% the bionanocomposite material exhibited a WU% value equals to $12.1\% \pm 0.3$, which is higher with respect to that of pristine polymer (8.2 ± 0.2) (Cavallaro et al., 2013). Regarding the mechanical performances of the films, we observed that the presence of HNT/CB[6] determines an improvement of both the elastic modulus and the tensile strength (Table 1) because of the adhesion of the pectin to the filler surface. Accordingly, the elongation at the breaking point decreased (Table 1) as a consequence of the pectin/nanofiller interactions that avoid the sliding of polymer chains against each other (Cavallaro et al., 2013).

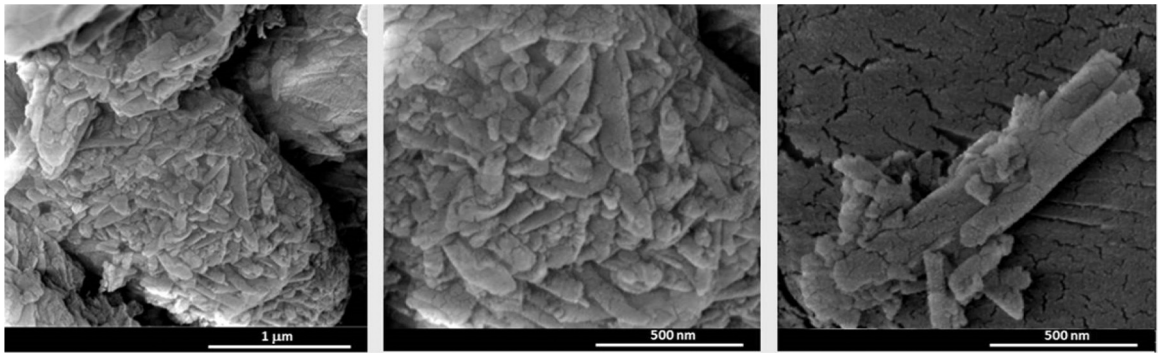

Fig. 5. SEM images of HNT/CB[6] nanofiller.

Table 1
Tensile properties of pectin and pectin + HNT/CB[6] films.

	Tensile strength/MPa	Elastic modulus/MPa	Elongation at the breaking point/%
Pectin[a]	2370 ± 4	41.6 ± 0.8	4.29 ± 0.02
Pectin + HNT/CB[6]	2991 ± 7	48.3 ± 1.2	2.05 ± 0.01

[a] From Cavallaro, Lazzara et al. (2011).

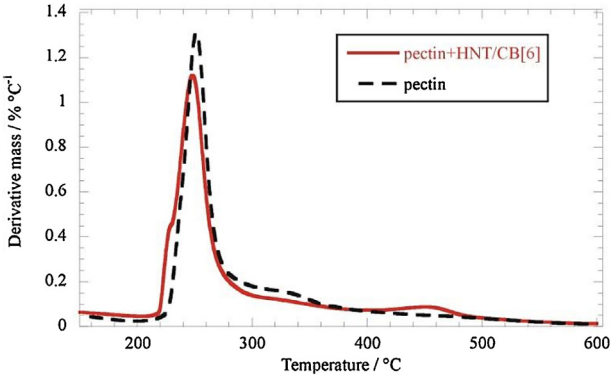

Fig. 6. DTG curves for pristine pectin and pectin + HNT/CB[6].

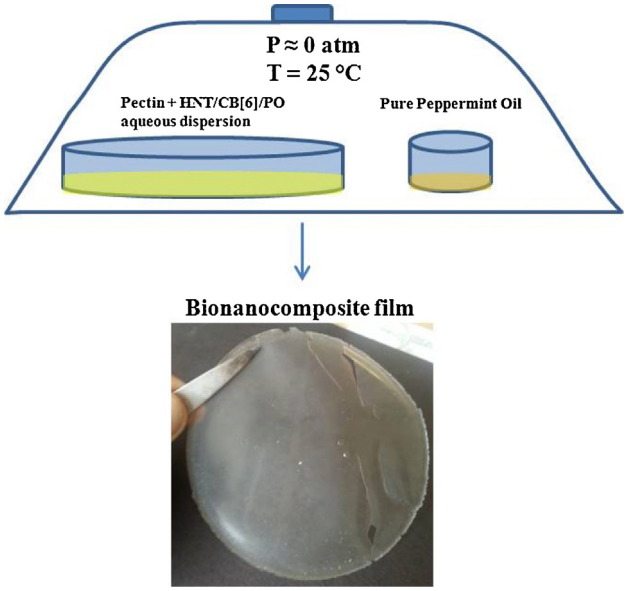

Fig. 7. Schematic representation of the apparatus for bionanocomposite preparation. The diameter of the Petri dish is 9 cm.

TG experiments highlighted that the pectin thermal behavior is slightly influenced by the presence of HNT/CB[6]. In particular, the polymer degradation temperature was estimated by the maximum of DTG curves in the temperature range between 200 and 400 °C (Fig. 6) where the pectin mainly degrades. We calculated that the polymer degradation temperatures are 249.7 °C and 248.5 °C for the pristine pectin and the bionanocomposite, respectively. Moreover, it should be noted that the DTG curve (Fig. 6) of pectin + HNT/CB[6] nanocomposite shows a peak centered at 453.8 °C, which is correlated to the CB[6] degradation. The corresponding weight loss endowed to estimate the CB[6] amount (1.7 wt%) in the nanocomposite film. This result is consistent with the CB[6] loading of modified HNT as well as the filler concentration (5 wt%) of the bionanocomposite. Therefore, neither the pectin/nanofiller interactions nor the casting preparation procedure influenced the composition of the HNT/CB[6] hybrid. On this basis, the modified HNT might be efficient in the encapsulation of essential oils even when dispersed in a pectin matrix endowed to prepare bionanocomposite films with antimicrobial and antioxidant properties.

3.2.2. Loading of peppermint oil into pectin + HNT/CB[6] biofilm

Due to the high volatility of essential oils, a "classic" casting method was not appropriate for the biofilm preparation. Therefore, an easy and cheap casting method under reduced pressure was realized in order to favor the PO entrapment into the bionanocomposite structure. As shown in Fig. 7, a Petri dish containing an aqueous mixture of pectin and HNT/CB[6]/PO was kept at saturated essential oil atmosphere in a vacuum desiccator jar lab. The biofilm obtained after the complete solvent evaporation appears optically transparent with a smooth surface (Fig. 7) in agreement with the low filler concentration. For comparison, a pectin based film was prepared by using the described procedure on a Petri dish containing a polymer/PO aqueous mixture with a 4:1 wt ratio.

3.2.3. Kinetic release

The action mechanism of functional films is related to the release of the incorporated agents into the surrounding headspace. Therefore, the antimicrobial and antioxidant efficiencies of the prepared biofilms are strictly correlated to both the extent and kinetics release of the essential oil. To this purpose, we investigated the release of menthone by means of HPLC experiments. It should be noted that menthone is the main component (24 wt%) of PO, which is a complex mixture of several organic compounds. Release studies were conducted at different temperatures by exposure of the films to a food simulant (50% v/v ethanol). Fig. 8a shows the release profiles (expressed as mg of menthone per cm^2 of film), which were successfully described by the first order exponential kinetic equation:

$$R = M_\infty \cdot (1 - e^{-kt}) \quad (3)$$

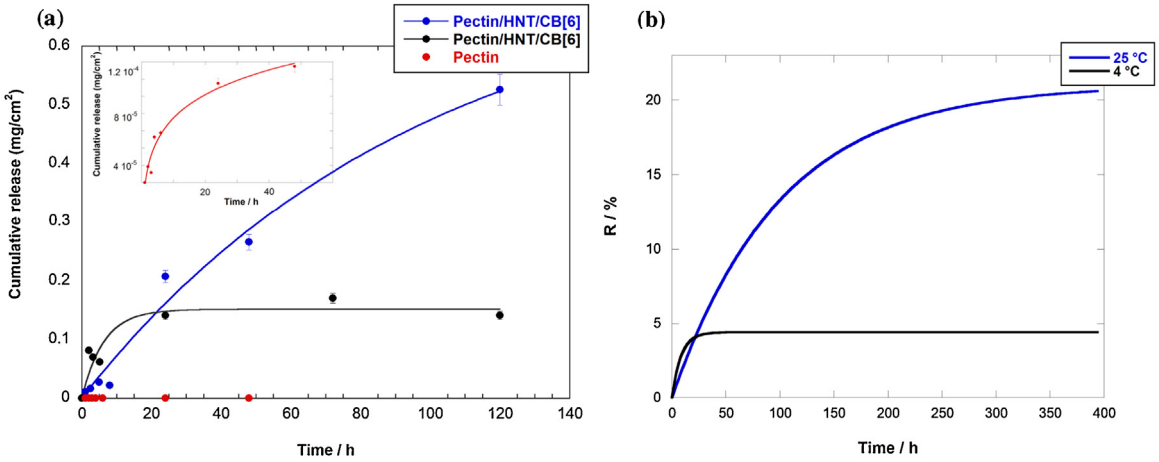

Fig. 8. Release profile of menthone from the pectin based films in 50% v/v ethanol (a). Red circles refer to pristine pectin at 25 °C (detail in the inset), while blue and black circles refer to the pectin + HNT/CB[6] nanocomposite at 25 and 4 °C, respectively. Solid lines represent the best fitting according to the Eq. (1). Percent of the menthone released on time (b) for the bionanocomposite film at 4 (black) and 25 °C (blue). (For interpretation of the references to colour in this figure legend, the reader is referred to the web version of this article.)

Table 2
Kinetic parameters for PO release into food simulant solvent.

	T (°C)	k (h^{-1})	M_∞ (mg cm^{-2})
Pectin	25	0.08 ± 0.02	$(1.2 \pm 0.1) \times 10^{-4}$
Pectin/HNT/CB[6]	25	0.010 ± 0.003	0.7 ± 0.1
Pectin/HNT/CB[6]	4	0.16 ± 0.05	0.15 ± 0.01

where M_∞ is the amount of active agent released at infinite time and k is the release rate constant.

Compared with the bionanocomposite film, pristine pectin releases a negligible amount of menthone at 25 °C, while the kinetics are very similar as evidenced by the k values (Table 2).

Interestingly, these results highlight that the HNT/CB[6] filler dispersed in the polymer matrix preserves the efficient adsorption capacity towards PO. As concerns the bionanocomposite film, both kinetics parameters are strongly dependent on the temperature. In particular, the menthone release is much slower at refrigeration temperature (4 °C) with respect to that observed at room temperature (25 °C). On the other hand, M_∞ values revealed that the temperature increase induces an enhancement of the total PO release highlighting that the mechanism action of the bionanocomposite is thermo-sensitive. These data could be due to the lower PO solubility in the selected solvent at lower temperatures. Based on the kinetics parameters, we estimated the percentage of menthone released on time (Fig. 8b) by taking into account the filler concentration in the film (5 wt%) as well as the PO loading ability of the HNT/CB[6] (60 wt%). Northwardly, PO is not fully released neither at 25 °C nor at 4 °C being that M_∞ values are 21 ± 4 and 4.3 ± 0.4 wt%, respectively. These results indicate that the bionanocomposite preserves its active agent in its structure even at higher temperatures. Therefore, the antimicrobial/antioxidant properties of the film could be tuned with the temperature driving to a multistep food conservation.

Tensile tests were carried out on the pectin + HNT/CB[6]/PO bionanocomposite after the exposure to the food simulant. Fig. 9 shows that the contact with ethanol (50% v/v) for 120 h generated a strong reduction of both the elastic modulus and the tensile strength, while the elongation at the breaking point significantly increased. These results reflect the plasticizing effect on the film that could be due to the sorption and diffusion of the solvent within the bionanocomposite structure. Such phenomenon was observed for the bioplastic film based on poly(3-hydroxybutyrate-*co*-3-hydroxyvalerate) (Chea, Angellier-Coussy, Peyron, Kemmer, & Gontard, 2016).

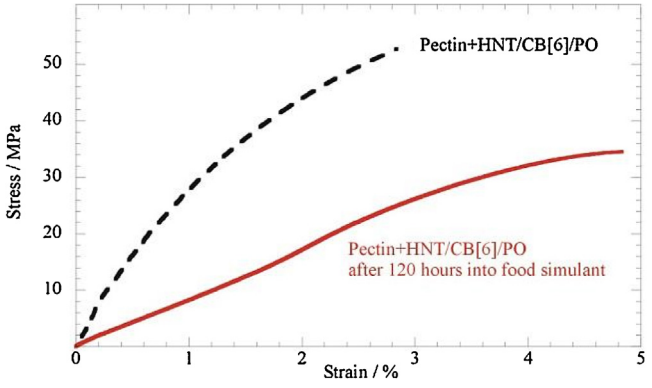

Fig. 9. Stress vs strain curves for the pectin + HNT/CB[6]/PO film before (black) and after (red) exposure to food simulant solvent. (For interpretation of the references to colour in this figure legend, the reader is referred to the web version of this article.)

Nevertheless, the mechanical performances of the biofilm are still adequate for food packaging. SEM images of the pectin + HNT/CB[6]/PO bionanocomposite highlighted that the exposure to the food simulant induces the formation of voids as a consequence of the solvent diffusion into the polymer structure. These findings agrees with the decrease of the mechanical performances (Fig. 10). Moreover, we observed the presence of several clusters (size ca. 4 μm) on the pectin surface because of the hydrophobic interactions between the modified nanotubes, which present CB[6] molecules on both inner and external surfaces.

3.2.4. DPPH radical scavenging activity

The radical trapping ability of PO was assessed by studying the reaction with 2,2-diphenyl-1-picrylhydrazyl radical (DPPH). The antioxidant capacity of PO in a mixture H_2O/EtOH (50% v/v) was evaluated by plotting the percentage of inhibition of the free radical scavenging capacity of DPPH against the concentrations of different standard solutions of PO (from 0.3 to 30 mg mL^{-1}) (see ESI). As expected, PO showed good antioxidant activity that enhances with the increasing of PO concentration (IC_{50} = 7.6 ± 0.2 mg mL^{-1}) while the pristine HNT did not exhibit any radical scavenging activity (Massaro, Amorati et al., 2016; Massaro, Riela, Guernelli et al., 2016). It should be noted that the antioxidant activity of

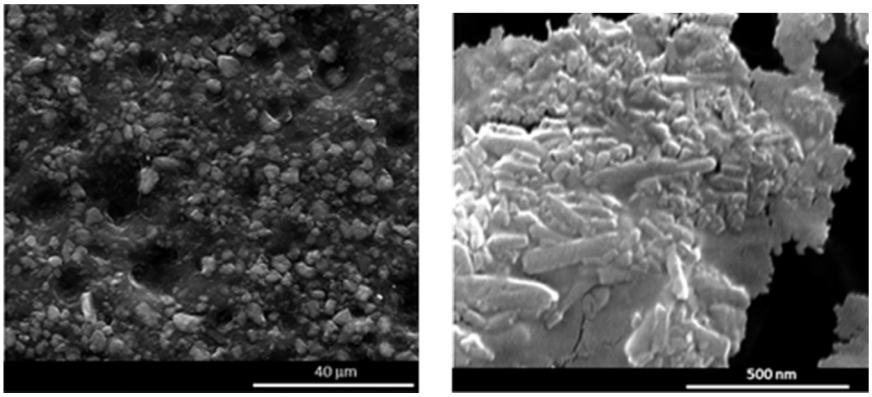

Fig. 10. SEM images of the film after the exposure to food simulant.

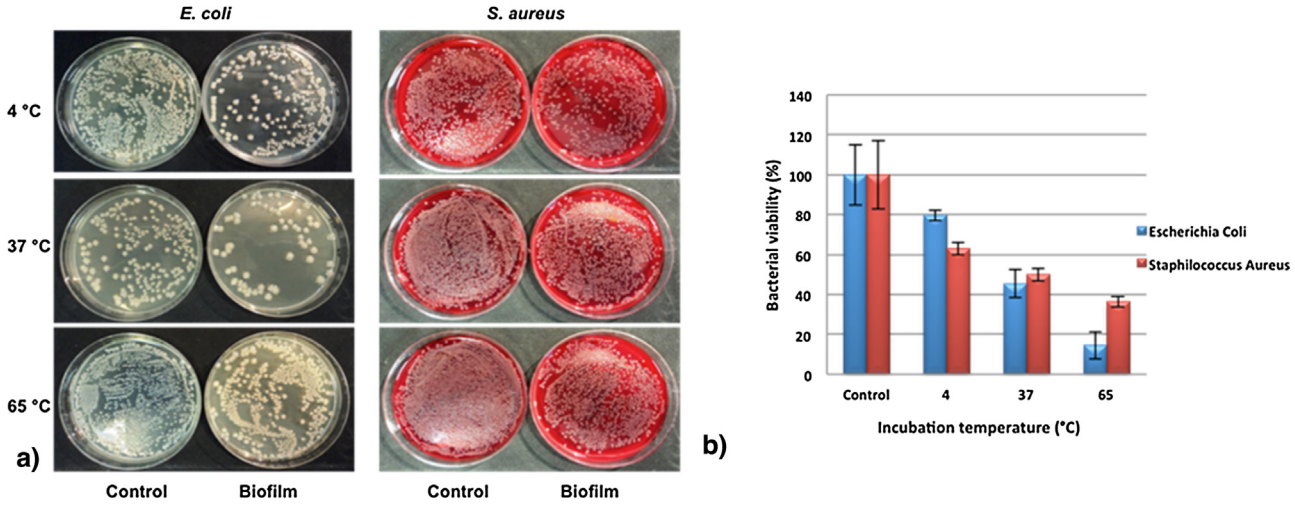

Fig. 11. Antibacterial activity of pectin/HNT/PO films against *E. coli* and *S. aureus* at 4, 37 and 65 °C incubated for 30 min.

the simulant exposed to pectin + HNT/CB[6]/PO film after 120 h was determined using the same DPPH method. The inhibition percentage of the free radical DPPH by PO released from the film was 41%. Therefore, the peppermint oil dispersed in the pectin + HNT/CB[6] film retains its reactivity toward radicals and therefore it can act as an antioxidant agent.

3.2.5. Antimicrobial activity

The in vitro antibacterial activity of pectin + HNT/CB[6]/PO film was determined against a Gram-negative bacteria *E. coli*, and a Gram-positive *S. aureus*, isolated by beef and cow milk, respectively. The activity of essential oils against pathogenic bacteria and their effects depends on their amount and on their chemical composition. Several mechanisms have been described to explain the activity of essential oils on bacterial cells. The membrane represents an efficient barrier between the external environment and the cytoplasm (Fortunati et al., 2014). In the presence of antimicrobial compounds, the bacteria may react altering the structure of the membrane. To measure the microbial viability of each bacterial strain, we employed a classic colony counting method following a procedure reported elsewhere with minor modifications (Higueras, López-Carballo, Gavara, & Hernández-Muñoz, 2014). Fig. 11 shows the viability (expressed as% bacterial viability) of *E. coli* and *S. aureus* cells onto pectin + HNT/CB[6]/PO films after incubation at three different temperatures; in particular, 4 °C and 65 °C were chosen to simulate the refrigeration and pasteurization conditions, respectively. Moreover, 37 °C was selected as an intermediate temperature.

Results showed that the cell viability for both bacterial strains on the biofilm without PO (control) was quite similar at each incubation temperature and they did not exhibit antimicrobial activity. Contrarily, the nanocomposite film loaded with PO showed a relevant antibacterial efficiency against *E. coli* and *S. aureus* strains that sre influenced by the incubation temperature ($p < 0.01$). The percentage of cell viability for both bacterial strains was reduced at 65 °C compared to those at 37 °C and 4 °C. Namely, the temperature increase (from 4 °C to 65 °C) induced a significant enhancement of the antibacterial activity. At a low temperature (4 °C) *E. coli* showed approximately 1.3-fold the survival rate respect to *S. aureus* (80% and 63%, respectively). As general result, the antimicrobial activity observed for *E. coli* at each incubation temperature was greater than *S. aureus*. It is noteworthy that only the 15% of *E. coli* survived after the treatment at 65 °C.

Interestingly, the reduced antibacterial activity of the pectin + HNT/CB[6]/PO film for *S. aureus* could be due to the molecular structure of the cell wall of Gram-positive respect to that of Gram-negative cells (Fortunati et al., 2014), where the presence of a thick peptidoglycane layer in the cell prevents the nanoparticles penetration. As a general result, the biological experiments showed that the antimicrobial activity against the two food-borne pathogens is thermo-sensitive. Interestingly, the action mechanism is significantly enhanced by temperature as demonstrated by the PO release experiments (Fig. 8). This finding confirms that the pectin filling with the HNT/CB[6]/PO

produces a nanocomposite film with thermo-tunable antimicrobial properties, which can be used for a multi-step food conservation.

4. Conclusions

The functionalization of halloysite nanotubes (HNT) with cucurbit[6]uril (CB[6]) molecules was achieved with the aim to develop a novel filler with a high solubilization capacity towards the peppermint essential oil (PO), which is an antioxidant and antimicrobial agent. The modification of HNT surfaces was successful as confirmed by thermogravimetry and IR spectroscopy, while SEM images showed that the tubular morphology is preserved in the functionalized filler. A significant enhancement (ca. 10 times) of the HNT adsorption ability towards PO was induced by the addition of CB[6] revealing that the hybrid filler is appropriate for the preparation of functional nanocomposites. On this basis, HNT/CB[6] loaded with the essential oil was filled into a pectin matrix by using the aqueous casting method under a vacuum as well as a PO saturated atmosphere. The addition of the hybrid filler enhanced both the mechanical performances and the surface hydrophobicity of the pectin based film, while the thermal behavior is slightly affected. Both the kinetics and the extent of PO released into the simulant food solvent (50% v/v ethanol) are thermo-sensitive. Interestingly, the bionanocomposite film preserves a large amount of the incorporated active agent at refrigerated as well as room temperature. In addition, the film maintains relevant mechanical peformances even after 120 h of exposure to the food simulant solvent. The biocomposite film showed a reliable antioxidant activity as evidenced by the large inhibition percentage (41%) of the free radical DPPH. As concerns the antimicrobial properties, in vitro experiments for *E. coli* (Gram-negative) and *S. aureus* (Gram-positive) isolated from food sources revealed that the composite biofilm is more efficient at higher temperatures confirming the PO release data. With this study, we successfully propose an easy strategy to prepare bionanocomposite films with a tunable antimicrobial activity on dependence of temperature driving to a multi-step food conservation. On this basis, the pectin + HNT/CB[6]/PO represents a potential and sustainable material for food packaging applications.

Author contributions

This manuscript was written through contributions by multiple authors. All authors have given their approval to the final version of the manuscript.

Acknowledgments

The authors are thankful to Dr. Gary Silcock. The work was financially supported by the University of Palermo (Italy), FIRB 2012 (prot. RBFR12ETL5) and PON-TECLA (PON03PE_00214_1).

Appendix A. Supplementary data

Supplementary data associated with this article can be found, in the online version, at http://dx.doi.org/10.1016/j.carbpol.2016.07.041.

References

Abdullayev, E., & Lvov, Y. (2013). Halloysite clay nanotubes as a ceramic skeleton for functional biopolymer composites with sustained drug release. *Journal of Materials Chemistry B*, *1*, 2894–2903.

Abdullayev, E., Price, R., Shchukin, D., & Lvov, Y. (2009). Halloysite tubes as nanocontainers for anticorrosion coating with benzotriazole. *ACS Applied Materials & Interfaces*, *1*, 1437–1443.

Abdullayev, E., Sakakibara, K., Okamoto, K., Wei, W., Ariga, K., & Lvov, Y. (2011). Natural tubule clay template synthesis of silver nanorods for antibacterial composite coating. *ACS Applied Materials & Interfaces*, *3*, 4040–4046.

Aguzzi, C., Cerezo, P., Viseras, C., & Caramella, C. (2007). Use of clays as drug delivery systems: Possibilities and limitations. *Applied Clay Science*, *36*, 22–36.

Alcantara, A. C. S., Aranda, P., Darder, M., & Ruiz-Hitzky, E. (2010). Bionanocomposites based on alginate-zein/layered double hydroxide materials as drug delivery systems. *Journal of Materials Chemistry*, *20*, 9495–9504.

Ali, S. S., Tang, X., Alavi, S., & Faubion, J. (2011). Structure and physical properties of starch/poly vinyl alcohol/sodium montmorillonite nanocomposite films. *Journal of Agricultural and Food Chemistry*, *59*, 12384–12395.

Arcudi, F., Cavallaro, G., Lazzara, G., Massaro, M., Milioto, S., Noto, R., et al. (2014). Selective Functionalization of Halloysite cavity by click reaction: Structured filler for enhancing mechanical properties of Bionanocomposite films. *The Journal of Physical Chemistry C*, *118*, 15095–15101.

Arfat, Y. A., Benjakul, S., Prodpran, T., Sumpavapol, P., & Songtipya, P. (2014). Properties and antimicrobial activity of fish protein isolate/fish skin gelatin film containing basil leaf essential oil and zinc oxide nanoparticles. *Food Hydrocolloids*, *41*, 265–273.

Bakry, A. M., Abbas, S., Ali, B., Majeed, H., Abouelwafa, M. Y., Mousa, A., et al. (2016). Microencapsulation of oils: A comprehensive review of benefits, techniques, and applications. *Comprehensive Reviews in Food Science and Food Safety*, *15*, 143–182.

Bellani, L., Giorgetti, L., Riela, S., Lazzara, G., Scialabba, A., & Massaro, M. (2016). Ecotoxicity of halloysite nanotubes supported palladium nanoparticles on Raphanus sativus L. *Environmental Toxicology and Chemistry*, http://dx.doi.org/10.1002/etc.3412

Beverlya, R. L., Janes, M. E., Prinyawiwatkula, W., & No, H. K. (2008). Edible chitosan films on ready-to-eat roast beef for the control of Listeria monocytogenes. *Food Microbiology*, *25*, 534–537.

Burt, S. (2004). Essential oils: Their antibacterial properties and potential applications in foods—a review. *International Journal of Food Microbiology*, *94*, 223–253.

Cavallaro, G., Lazzara, G., & Milioto, S. (2012). Exploiting the colloidal stability and solubilization ability of clay nanotubes/ionic surfactant hybrid nanomaterials. *The Journal of Physical Chemistry C*, *116*, 21932–21938.

Cavallaro, G., Lazzara, G., & Milioto, S. (2013). Sustainable nanocomposites based on halloysite nanotubes and pectin/polyethylene glycol blend. *Polymer Degradation and Stability*, *98*, 2529–2536.

Cavallaro, G., Donato, D. I., Lazzara, G., & Milioto, S. (2011). Films of halloysite nanotubes sandwiched between two layers of biopolymer: From the morphology to the dielectric, thermal, transparency, and wettability properties. *The Journal of Physical Chemistry C*, *115*, 20491–20498.

Cavallaro, G., Lazzara, G., & Milioto, S. (2011). Dispersions of nanoclays of different shapes into aqueous and solid biopolymeric matrices. Extended physicochemical study. *Langmuir*, *27*, 1158–1167.

Chea, V., Angellier-Coussy, H., Peyron, S., Kemmer, D., & Gontard, N. (2016). Poly(3-hydroxybutyrate-*co*-3-hydroxyvalerate) films for food packaging: Physical–chemical and structural stability under food contact conditions. *Journal of Applied Polymer Science*, *133*

Coffin, D. R., & Fishman, M. L. (1994). Physical and mechanical properties of highly plasticized pectin/starch films. *Journal of Applied Polymer Science*, *54*, 1311–1320.

Coffin, D. R., Fishman, M. L., & Ly, T. V. (1996). Thermomechanical properties of blends of pectin and poly(vinyl alcohol). *Journal of Applied Polymer Science*, *61*, 71–79.

Espitia, P. J. P., Du, W.-X., Avena-Bustillos, R. d. J., Soares, N. d. F. F., & McHugh, T. H. (2014). Edible films from pectin: Physical-mechanical and antimicrobial properties—a review. *Food Hydrocolloids*, *35*, 287–296.

Fakhrullina, G. I., Akhatova, F. S., Lvov, Y. M., & Fakhrullin, R. F. (2015). Toxicity of halloysite clay nanotubes in vivo: A Caenorhabditis elegans study. *Environmental Science: Nano*, *2*, 54–59.

Farris, S., Schaich, K. M., Liu, L., Cooke, P. H., Piergiovanni, L., & Yam, K. L. (2011). Gelatin–pectin composite films from polyion-complex hydrogels. *Food Hydrocolloids*, *25*, 61–70.

Fortunati, E., Rinaldi, S., Peltzer, M., Bloise, N., Visai, L., Armentano, I., et al. (2014). Nano-biocomposite films with modified cellulose nanocrystals and synthesized silver nanoparticles. *Carbohydrate Polymers*, *101*, 1122–1133.

Garcíía, M. a. A., Pinotti, A., Martino, M. N., & Zaritzky, N. E. (2004). Characterization of composite hydrocolloid films. *Carbohydrate Polymers*, *56*, 339–345.

Gorrasi, G. (2015). Dispersion of halloysite loaded with natural antimicrobials into pectins: Characterization and controlled release analysis. *Carbohydrate Polymers*, *127*, 47–53.

Higueras, L., López-Carballo, G., Gavara, R., & Hernández-Muñoz, P. (2014). Reversible covalent immobilization of cinnamaldehyde on chitosan films via Schiff base formation and their application in active food packaging. *Food and Bioprocess Technology*, *8*, 526–538.

Iturriaga, L., Olabarrieta, I., Castellan, A., Gardrat, C., & Coma, V. (2014). Active naringin-chitosan films: Impact of UV irradiation. *Carbohydrate Polymers*, *110*, 374–381.

Kim, J., Jung, I.-S., Kim, S.-Y., Lee, E., Kang, J.-K., Sakamoto, S., et al. (2000). New cucurbituril homologues: Syntheses, isolation, characterization, and X-ray crystal structures of cucurbit[n]uril (n = 5, 7, and 8). *Journal of the American Chemical Society*, *122*, 540–541.

Kryuchkova, M., Danilushkina, A., Lvov, Y., & Fakhrullin, R. (2016). Evaluation of toxicity of nanoclays and graphene oxide in vivo: A Paramecium caudatum study. *Environmental Science: Nano*, *3*, 442–452.

Lee, M. H., & Park, H. J. (2015). Preparation of halloysite nanotubes coated with Eudragit for a controlled release of thyme essential oil. *Journal of Applied Polymer Science*, *132*.
Liu, M., Wu, C., Jiao, Y., Xiong, S., & Zhou, C. (2013). Chitosan-halloysite nanotubes nanocomposite scaffolds for tissue engineering. *Journal of Materials Chemistry B*, *1*, 2078–2089.
Lun, H., Ouyang, J., & Yang, H. (2014). Natural halloysite nanotubes modified as an aspirin carrier. *RSC Advance*, *4*, 44197–44202.
Luo, Z., Song, H., Feng, X., Run, M., Cui, H., Wu, L., et al. (2013). Liquid crystalline phase behavior and sol–gel transition in aqueous halloysite nanotube dispersions. *Langmuir*, *29*, 12358–12366.
Lvov, Y., & Abdullayev, E. (2013). Functional polymer–clay nanotube composites with sustained release of chemical agents. *Progress in Polymer Science*, *38*, 1690–1719.
Lvov, Y. M., Shchukin, D. G., Möhwald, H., & Price, R. R. (2008). Halloysite clay nanotubes for controlled release of protective agents. *ACS Nano*, *2*, 814–820.
Lvov, Y. M., DeVilliers, M. M., & Fakhrullin, R. F. (2016). The application of halloysite tubule nanoclay in drug delivery. *Expert Opinion on Drug Delivery*, 1–10.
Lvov, Y., Wang, W., Zhang, L., & Fakhrullin, R. (2016). Halloysite clay nanotubes for loading and sustained release of functional compounds. *Advanced Materials*, *28*, 1227–1250.
Márquez, C., Hudgins, R. R., & Nau, W. M. (2004). Mechanism of host-guest complexation by cucurbituril. *Journal of the American Chemical Society*, *126*, 5806–5816.
Machado, G. S., de Freitas Castro, K. A. D., Wypych, F., & Nakagaki, S. (2008). Immobilization of metalloporphyrins into nanotubes of natural halloysite toward selective catalysts for oxidation reactions. *Journal of Molecular Catalysis A: Chemical*, *283*, 99–107.
Manso, S., Becerril, R., Nerín, C., & Gómez-Lus, R. (2015). Influence of pH and temperature variations on vapor phase action of an antifungal food packaging against five mold strains. *Food Control*, *47*, 20–26.
Marmur, A. (2008). From hygrophilic to superhygrophobic: Theoretical conditions for making high-contact-angle surfaces from low-contact-angle materials. *Langmuir*, *24*, 7573–7579.
Massaro, M., Riela, S., Cavallaro, G., Gruttadauria, M., Milioto, S., Noto, R., et al. (2014). Eco-friendly functionalization of natural halloysite clay nanotube with ionic liquids by microwave irradiation for Suzuki coupling reaction. *Journal of Organometallic Chemistry*, *749*, 410–415.
Massaro, M., Amorati, R., Cavallaro, G., Guernelli, S., Lazzara, G., Milioto, S., et al. (2016). Direct chemical grafted curcumin on halloysite nanotubes as dual-responsive prodrug for pharmacological applications. *Colloids and Surfaces B: Biointerfaces*, *140*, 505–513.
Massaro, M., Piana, S., Colletti, C. G., Noto, R., Riela, S., Baiamonte, C., et al. (2015). Multicavity halloysite-amphiphilic cyclodextrin hybrids for co-delivery of natural drugs into thyroid cancer cells. *Journal of Materials Chemistry B*, *3*, 4074–4081.
Massaro, M., Riela, S., Cavallaro, G., Colletti, C. G., Milioto, S., Noto, R., et al. (2015). Palladium supported on Halloysite-triazolium salts as catalyst for ligand free Suzuki cross-coupling in water under microwave irradiation. *Journal of Molecular Catalysis A: Chemical*, *408*, 12–19.
Massaro, M., Riela, S., Cavallaro, G., Colletti, C. G., Milioto, S., Noto, R., et al. (2016). Ecocompatible halloysite/cucurbit[8]uril hybrid as efficient nanosponge for pollutants removal. *ChemistrySelect*, *1*, 1773–1779.
Massaro, M., Riela, S., Guernelli, S., Parisi, F., Lazzara, G., Baschieri, A., et al. (2016). A synergic nanoantioxidant based on covalently modified halloysite-trolox nanotubes with intra-lumen loaded quercetin. *Journal of Materials Chemistry B*, *4*, 2229–2241.
Pasbakhsh, P., Churchman, G. J., & Keeling, J. L. (2013). Characterisation of properties of various halloysites relevant to their use as nanotubes and microfibre fillers. *Applied Clay Science*, *74*, 47–57.
Průšová, A., Šmejkalová, D., Chytil, M., Velebný, V., & Kučerík, J. (2010). An alternative DSC approach to study hydration of hyaluronan. *Carbohydrate Polymers*, *82*, 498–503.
Shutava, T. G., Fakhrullin, R. F., & Lvov, Y. M. (2014). Spherical and tubule nanocarriers for sustained drug release. *Current Opinion in Pharmacology*, *18*, 141–148.
Sorrentino, A., Gorrasi, G., & Vittoria, V. (2007). Potential perspectives of bio-nanocomposites for food packaging applications. *Trends in Food Science & Technology*, *18*, 84–95.
Suh, Y. J., Kil, D. S., Chung, K. S., Abdullayev, E., Lvov, Y. M., & Mongayt, D. (2011). Natural nanocontainer for the controlled delivery of glycerol as a moisturizing agent. *Journal of Nanoscience and Nanotechnology*, *11*, 661–665.
Szczepanik, B., & Słomkiewicz, P. (2016). Photodegradation of aniline in water in the presence of chemically activated halloysite. *Applied Clay Science*, *124–125*, 31–38.
Talja, R. A., Peura, M., Serimaa, R., & Jouppila, K. (2008). Effect of amylose content on physical and mechanical properties of potato-starch-based edible films. *Biomacromolecules*, *9*, 658–663.
Tescione, F., Buonocore, G. G., Stanzione, M., Oliviero, M., & Lavorgna, M. (2014). Controlling the release of active compounds from the inorganic carrier halloysite. *AIP Conference Proceedings*, *1599*, 446–449.
Wei, W., Minullina, R., Abdullayev, E., Fakhrullin, R., Mills, D., & Lvov, Y. (2014). Enhanced efficiency of antiseptics with sustained release from clay nanotubes. *RSC Advance*, *4*, 488–494.
Zhang, Z., Zhang, R., Zou, L., Chen, L., Ahmed, Y., Al Bishri, W., et al. (2016). Encapsulation of curcumin in polysaccharide-based hydrogel beads: Impact of bead type on lipid digestion and curcumin bioaccessibility. *Food Hydrocolloids*, *58*, 160–170.
Zhu, J., He, H., Zhu, L., Wen, X., & Deng, F. (2005). Characterization of organic phases in the interlayer of montmorillonite using FTIR and 13C NMR. *Journal of Colloid and Interface Science*, *286*, 239–244.